Macromolecules

ARTICLE

pubs.acs.org/Macromolecules

Effects of Temperature and Polymer Composition upon the Aqueous Solution Properties of Comblike Linear Poly(ethylene imine)/Poly(2-ethyl-2-oxazoline)-Based Polymers

Silvia Halacheva,*[,†] Gareth J. Price,[‡] and Vasil M. Garamus[§]

[†]Physical and Theoretical Chemistry Laboratory, University of Oxford, South Parks Road, Oxford, OX1 3QZ, United Kingdom

[‡]Department of Chemistry, University of Bath, Claverton Down, Bath, BA2 7AY, United Kingdom

[§]Helmholtz-Zentrum Geesthacht: Zentrum für Material und Küstenforschung GmbH, Max Planck Strasse 1, D-21502, Geesthacht, Germany

Supporting Information

ABSTRACT: A range of well-defined, sparsely grafted, comblike linear poly(ethylene imine)/poly(2-ethyl-2-oxazoline) (LPEI-*comb*-PEtOx) and comblike linear poly(ethylene imine)/linear poly(ethylene imine) (LPEI-*comb*-LPEI) polymers with various degrees of polymerization of both main and side chains were prepared. Their aqueous solution properties were investigated by means of dynamic light scattering (DLS) and small-angle neutron scattering (SANS) over a temperature range of 25−65 °C. For LPEI-*comb*-LPEI polymers the particle distributions were mono-, bi-, or trimodal depending upon the temperature and/or polymer composition. The particles tended to decrease in size upon heating due to the weakening of intra- and interchain hydrogen bonds between −NH groups of the polymers and also with water molecules. However, the aggregates formed from the LPEI-*comb*-LPEI polymers featuring longer main chains, shorter branches, and lower grafting densities were more resistant to heat-induced disassociation. LPEI-*comb*-PEtOx particles featured smoother temperature variations of hydrodynamic radius and typically bimodal distributions. The shape and structure of the small LPEI-*comb*-PEtOx aggregates (average radius ∼6 nm) as well as their temperature evolution were studied by SANS. A variety of structures were observed, depending upon the polymer composition. The LPEI-*comb*-PEtOx polymers with low grafting densities and short branches formed elongated aggregates, whereas particles of spherical core−shell structure were observed for the more densely grafted polymer with longer branches. Spherical or rodlike aggregates were monitored in LPEI-*comb*-LPEI aqueous solutions.

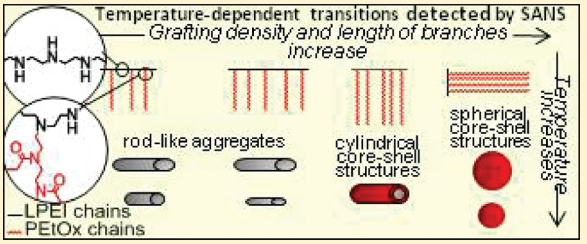

INTRODUCTION

Stimuli-responsive materials constitute a rapidly growing field of interest in polymer and colloid science due to their ability to undergo sharp changes in their physical properties as a result of small variations in external conditions such as temperature, light, salt concentration, ionic strength, and pH.[1−4] Recently, amphiphilic copolymers have attracted considerable attention because of their advantageous physical properties in the context of biomedical and nanotechnological applications such as drug delivery, cell encapsulation, and tissue engineering.[5−11] When these materials are dissolved in a selective solvent, micelles of various morphologies may be formed.

Recent molecular dynamic simulations and theoretical predictions of the self-assembled structures formed from amphiphilic comblike copolymers upon poor solvent quality for the backbone reveal that the sequence of morphological transitions is governed by a balance between repulsive interactions among the branches and the solvophobic interactions of the main chain.[12−14] The formation of a "pearl necklace" structure, comprised of multiple spherical micelles in solution, which are stabilized by steric repulsion between coronas, has been reported for copolymers which have a sufficiently dense level of grafting. In the case of sparsely grafted copolymers, however, the formation of intramolecular aggregates of diverse morphology including pearl necklaces of spherical micelles, unimolecular wormlike cylindrical micelles, and also disk-shaped, lamellar-like intramolecular aggregates were suggested.[13]

Our research is focused on the cationic polyelectrolyte poly(ethylene imine) (PEI), which has been recently recognized as one of the most efficient nonviral vectors for *in vivo* and *in vitro* transfections. At low pH, linear PEI (LPEI) is extensively protonated (at pH 2.4, ∼70% of the amino groups are positively charged, and at pH 7 this proportion decreases to 30%), whereas at high pH it is an essentially neutral polymer (at pH 10, ∼4% are positively charged).[15−17] Commercially available PEI is a highly branched, water-soluble polymer which is usually prepared via cationic ring-opening polymerization of ethylene imine. LPEI can be produced by the living cationic ring-opening polymerization

Received: June 7, 2011
Revised: August 15, 2011
Published: August 26, 2011

dx.doi.org/10.1021/ma2012859 | *Macromolecules* 2011, 44, 7394–7404

of 2-ethyl-2-oxazoline (EtOx),[18,19] followed by alkaline or acidic hydrolysis of the resulting PEtOx.[20−24] LPEI exhibits markedly different solubility properties compared with the commercially available, highly branched PEI. Because of its linear and flexible backbone, LPEI is insoluble in water at room temperature but dissolves when heated.[24] Moreover, LPEI has been found to adopt a double-stranded helix structure in the solid state, when free from traces of moisture.[25−28] Upon introduction of water molecules into the crystal lattice, a planar-zigzag conformation is adopted. Thermal effects upon the crystalline structure of LPEI in water have also been investigated.[29,30] The solubility change was attributed to the thermal induced conformational transition from the planar-zigzag form to random coil one, followed by hydration. In the heating/cooling cycle large hysteresis, attributed to the formation of intermolecular hydrogen bonds, has been observed. The cloud points seen in solutions of LPEI have been directly related to the polymer's melting point and the degree of polymerization.[22]

Several copolymers of other thermosensitive blocks with PEI have been explored in order to modify its cytotoxicity and transfection efficiency and their response to stimuli in solution.[31−35] Our study has focused on the solution properties of LPEI-*comb*-PEtOx copolymers comprised of a LPEI backbone with hydrophilic PEtOx branches. PEtOx has been identified as a biocompatible polymer, with even faster blood clearance than poly(ethylene oxide) (PEO), which makes it especially attractive for a variety of biomedical applications.[36,37] Furthermore, a cloud point temperature of around 61−64 °C, which can be tuned by varying the degree of polymerization, polymer composition, and concentration, was found for PEtOx polymers with molecular weights ranging from 20 to 500 kDa.[36,38] It has also been reported that PEtOx with a molecular weight below 10 kDa does not exhibit a cloud point.[39,40]

Quantitative deacylation of LPEI-*comb*-PEtOx to prepare LPEI-*comb*-LPEI polymers has been reported.[41,42] In contrast to LPEI-*comb*-PEtOx, LPEI-*comb*-LPEI consists of insoluble branches as well as an insoluble polymer backbone (at room temperature), and to the best of our knowledge, the thermal and aqueous solution properties of these polymers remain unstudied.

Herein, we aim to quantify the physicochemical changes and possible phase transitions of the comblike polymers LPEI-*comb*-PEtOx and LPEI-*comb*-LPEI in water in order to achieve a more fundamental understanding of their solution phase behaviors. The effect of the main and side chain lengths, as well as the grafting density on the aggregates formed from the various LPEI-based comblike polymers in aqueous solution, has been studied as a function of temperature using dynamic light scattering and small-angle neutron scattering.

EXPERIMENTAL SECTION

A. Materials. All glassware was dried at 150 °C overnight and assembled under a stream of dry nitrogen. 2-Ethyl-2-oxazoline (Aldrich) was distilled from calcium hydride. Methyl *p*-toluenesulfonate (Aldrich) was purified via vacuum distillation. Acetonitrile (Aldrich, 99.8%) anhydrous, tetrahydrofuran (Aldrich, 99.9+%, HPLC grade), anhydrous dichloromethane (Aldrich, ≥99.8%), and anhydrous diethyl ether (Aldrich, ≥99%) were used without further purification. Hydrochloric acid (32%) was purchased from Fisher Scientific. Dialysis tubing (Medicell International Ltd.) with cutoff in the range from 3.5 to 20 kDa was used for the separation of LPEI-*comb*-PEtOx comblike polymers from unreacted PEtOx. Deuterium oxide (Aldrich) and high-purity water (Elga Ultrapure) were used throughout.

B. Polymerizations. *Synthesis of PEtOx.* The following procedure for the synthesis of $PEtOx_{66}$ is representative. 2-Ethyl-2-oxazoline (8.33 g, 84 mmol) was added to a solution of methyl *p*-toluenesulfonate (220 mg, 1.18 mmol) in 100 mL of acetonitrile, aiming to obtain PEtOx with a degree of polymerization of 71. The reaction mixture was stirred at reflux for 144 h and then cooled to room temperature. After evaporation of the solvent under reduced pressure, the residual solid was dissolved in anhydrous dichloromethane and precipitated in cold diethyl ether. After filtration, the product was dried under vacuum, yielding 7.2 g (93%) of $PEtOx_{66}$ (determined by ^{1}H NMR) as a yellow powder. The other $PEtOx_n$ polymers were obtained by altering the ratio of monomer (EtOx) to initiator (TsOMe).

Synthesis of LPEI. The following procedure for the synthesis of $LPEI_{96}$ is representative. $PEtOx_{96}$ (1.00 g, 0.105 mmol) was dissolved in 4.7 M $HCl_{(aq)}$ (5 mL) and heated at 100 °C for 12 h. After cooling to room temperature, the acid/water was evaporated under reduced pressure. The resulting solid was redissolved in water and the pH adjusted to 8−9 by addition of 2.5 M $NaOH_{(aq)}$ solution. The resulting precipitate was filtered and washed thoroughly with deionized water. The remaining water was removed by freeze-drying to afford the product as a white powder.

Synthesis of LPEI-comb-PEtOx. The following procedure for the synthesis of $LPEI_{20}$-*comb*$_{20}$-$PEtOx_{96}$ copolymer (the coding of samples is described below) is representative. In a separate flask, $PEtOx_{96}$ was synthesized by initiating EtOx (10.0 g, 101 mmol) with methyl *p*-toluenesulfonate (0.19 g, 1.02 mmol) in 100 mL of acetonitrile. To the solution of living $PEtOx_{96}$, a hot solution of the initiator core $LPEI_{20}$ (dried by azeotropic distillation) in toluene was added. In this case, the molar ratio of oligomer PEtOx chains to secondary amine groups (on the LPEI core) was one. The mixture was refluxed for 8 h, during which time the LPEI-*comb*-PEtOx formed a separate liquid phase. After cooling to room temperature, the comblike polymer was dissolved in anhydrous dichloromethane and precipitated in cold diethyl ether. Ungrafted PEtOx oligomers were removed by dialysis (20 kDa MWCO) against deionized water. Finally, water was removed from the polymer by freeze-drying.

Synthesis of LPEI-comb-LPEI. The following procedure for the synthesis of $LPEI_{20}$-*comb*$_{20}$-$LPEI_{96}$ is representative. The resulting $LPEI_{20}$-*comb*$_{20}$-$PEtOx_{96}$ copolymers were hydrolyzed by heating in 4.7 M $HCl_{(aq)}$ at 90 °C overnight. After cooling to room temperature, the pH was adjusted to 9−10 by slow addition of 2.5 M aqueous NaOH solution. The mixture was then heated to reflux under a nitrogen atmosphere, and the product formed an oily layer on the surface of the solution, which became solid upon cooling. It was removed and redissolved in 600 mL of boiling water. This mixture was allowed to cool, and a white suspension was obtained. After ultracentrifugation at 8000 rpm for 10 min, the clear liquid was decanted, and the white precipitate dried via azeotropic distillation with toluene in a Dean−Stark apparatus to afford the title compound as a white solid.

C. Preparation of Polymer Solutions. Aqueous solutions of LPEI-*comb*-PEtOx were prepared by dilution of stock solutions prepared gravimetrically by adding water/D_2O to a preweighed quantity of the copolymer and mixing overnight under gentle mechanical agitation. LPEI-*comb*-LPEI and LPEI aqueous solutions were heated to 60 °C before the addition of the appropriate quantity of water/D_2O. DLS and SANS measurements were performed with dilute[43−45] polymer solutions (3.75 mg mL^{-1}), to which no other compounds were added. The pH values of the solutions were approximately 7.5 for LPEI-*comb*-PEtOx and 9 for LPEI-*comb*-LPEI.

D. Analysis. *Gel Permeation Chromatography (GPC).* GPC was performed using a PL-GPC50 system with tetrahydrofuran as eluent at a flow rate of 1.0 mL min^{-1}. Samples were prepared as solutions

Table 1. Characterization Data for PEtOx and LPEI Polymers

PEtOx					LPEI		
DP							
theor	exp[a]	dispersity by GPC	M_n[a]	code	DP[b]	M_n[b]	code
20	20	1.1	2000	$PEtOx_{20}$	20	860	$LPEI_{20}$
50	48	1.2	4800	$PEtOx_{48}$	48	2100	$LPEI_{48}$
71	66	1.3	6600	$PEtOx_{66}$	66	2900	$LPEI_{66}$
99	96	1.2	9600	$PEtOx_{96}$	96	4200	$LPEI_{96}$

[a] Determined by ^{1}H NMR ($CDCl_3$). [b] Determined by ^{1}H NMR (D_2O, 60 °C).

in tetrahydrofuran. Calibration was performed with polystyrene standards.

Proton Nuclear Magnetic Resonance (^{1}H NMR). ^{1}H NMR spectra were recorded at 400 MHz on a Bruker ICON NMR spectrometer. The samples were prepared as solutions in $CDCl_3$ or D_2O. The chemical shifts (δ) are quoted in ppm and are referenced to the residual solvent peak.

Dynamic Light Scattering (DLS). The light scattering photometer consists of a 50 mW He/Ne laser, operating at 633 nm with a standard avalanche photodiode (APD) and 90° detection optics connected to a Malvern Zetasizer Nano S90 autocorrelator. The quartz glass cylindrical cuvette was sealed and then immersed in a temperature controlled cell holder. Hydrodynamic radii (R_h, in nm) of the polymers were measured at 90°. At least 10 correlation functions were analyzed per sample, at each temperature, in order to obtain an average measurement.

Small-Angle Neutron Scattering (SANS). The SANS experiments were performed at the SANS1 instrument at the FRG1 research reactor at Helmholtz-Zentrum Geesthacht: Zentrum für Material and Küstenforschung GmbH, Geesthacht, Germany.[46] The range of scattering vectors q from 0.05 to 2.6 nm^{-1} was covered by four sample-to-detector distances (from 0.7 to 9.7 m). The neutron wavelength was 0.81 nm, and the wavelength spread of the mechanical velocity selector was 10% (fwhm). The samples were kept in quartz cells (Helma, Germany) with a path length of 2 mm. For isothermal conditions, a thermostated sample holder was used. The raw spectra were corrected for background signals from the solvent (D_2O), sample cell, and other sources by conventional procedures. The two-dimensional isotropic scattering spectra were azimuthally averaged, converted to absolute scale, and corrected for detector efficiency by dividing by the incoherent scattering spectrum of pure water, which was measured with a 1 mm path length quartz cell. The smearing induced by the different instrumental settings was included in the data analysis.[47]

RESULTS AND DISCUSSION

Synthesis and Characterization of PEtOx and LPEI Polymers. The living character of the cationic ring-opening polymerization of EtOx has been extensively investigated and reviewed.[18,19,36] In this work, the strong electrophile methyl *p*-toluenesulfonate was employed to initiate the polymerization of EtOx. A number of polymerizations were carried out (Table 1) aiming to prepare polymers with degrees of polymerization (DPs) from 20 to 99.

The PEtOx polymers were characterized by GPC and ^{1}H NMR. The polymer characterization data are shown in the Supporting Information. GPC analyses gave monomodal distributions with dispersity indices ranging from 1.1 to 1.3. The DPs of the PEtOx were estimated from the ^{1}H NMR spectra of the polymers in $CDCl_3$. The experimental DPs are in good agreement with the theoretical values and with those calculated from the feed (Table 1).

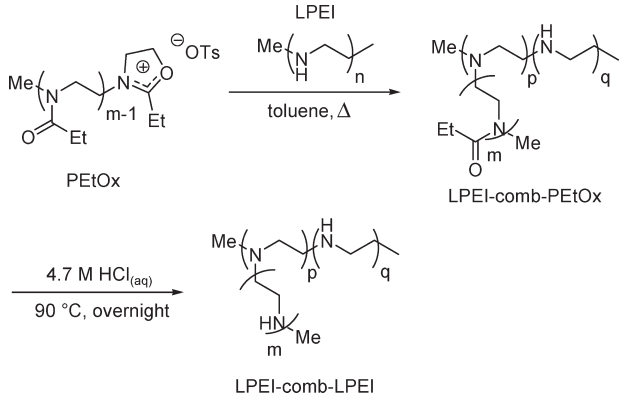

Figure 1. Synthesis of LPEI-*comb*-PEtOx and LPEI-*comb*-LPEI polymers (where $p + q = n$).

LPEI was obtained by acidic hydrolysis of PEtOx. It was reported previously that the degree of deacylation of PEtOx could be controlled by the amount of acid used.[21] To facilitate the complete hydrolysis, an excess of acid was employed. Examination of the ^{1}H NMR spectra revealed the degree of hydrolysis to be >95%. The DP of the resulting LPEI was confirmed as equivalent to that of the corresponding PEtOx precursors (see Supporting Information).

Synthesis of LPEI-*comb*-PEtOx and LPEI-*comb*-LPEI Polymers. The LPEI-*comb*-PEtOx and LPEI-*comb*-LPEIs were synthesized by a comb-burst branching strategy, as utilized by Tomalia.[41,42] Recently, this method has been successfully applied by Aoi[48] to obtain chitin derivatives featuring PEtOx side chains. The technique involves the grafting of PEtOx chains onto a LPEI "initiator core" in order to produce comb-branched LPEI-*comb*-PEtOx copolymers. These compounds were then hydrolyzed in order to obtain the final LPEI-*comb*-LPEI products. In particular, the reaction involves the quenching of the living PEtOx oligomers onto secondary amines of LPEI resulting in LPEI-*comb*-PEtOx in good yields (Figure 1). This strategy allows significant control of the critical molecular design parameters, such as size, shape, surface chemistry, and topology. For example, when the blocks of LPEI are particularly long, rod-type morphology can be expected, whereas spherical forms are favored when the blocks are shorter. A number of polymerizations were carried out, aiming to prepare sparsely grafted comblike polymers with random graft positions and with varying chain lengths of both LPEI backbone and PEtOx branches. The polymer compositions and degrees of grafting (DG) were determined from the ^{1}H NMR spectra in D_2O (see Supporting Information). This data are presented in Table 2. All comblike polymers have also been characterized by solid-state Fourier transform infrared (FTIR) spectroscopy. The transmittance FTIR spectra of some of the solid LPEI-*comb*-PEtOx and LPEI-*comb*-LPEI polymers are shown elsewhere.[49] The structure of LPEI-*comb*-PEtOx and the final LPEI-*comb*-LPEI polymers is schematically presented in Figure 2.

Dynamic Light Scattering. In this section we consider the solution properties of sparsely grafted LPEI-*comb*-PEtOx and LPEI-*comb*-LPEI copolymers in water. For comparison purposes, the solution behavior of the related LPEI polymers was studied as well. For LPEI-*comb*-PEtOx, water is a poor solvent for the main chain at ambient temperatures but efficiently solvates

Table 2. Characterization data for LPEI-*comb*-PEtOx and LPEI-*comb*-LPEI Polymers

DP of main chain ($LPEI_n$)[a]	DP of branches ($PEtOx_n$)[a]	DG[b] (%)	LPEI content in LPEI-*comb*-PEtOx (mol %)	code LPEI-*comb*-PEtOx	code LPEI-*comb*-LPEI
66	48	4	34	$LPEI_{66}$-$comb_4$-$PEtOx_{48}$	$LPEI_{66}$-$comb_4$-$LPEI_{48}$
96	48	5	29	$LPEI_{96}$-$comb_5$-$PEtOx_{48}$	$LPEI_{96}$-$comb_5$-$LPEI_{48}$
66	66	7	18	$LPEI_{66}$-$comb_7$-$PEtOx_{66}$	$LPEI_{66}$-$comb_7$-$LPEI_{66}$
20	96	20	5	$LPEI_{20}$-$comb_{20}$-$PEtOx_{96}$	$LPEI_{20}$-$comb_{20}$-$LPEI_{96}$

[a] Determined from ^{1}H NMR spectra of PEtOx and LPEI precursors (see Table 1). [b] Determined from ^{1}H NMR spectra of LPEI-*comb*-PEtOx in D_2O at 60 °C; the data are in agreement with that previously reported.[32,50]

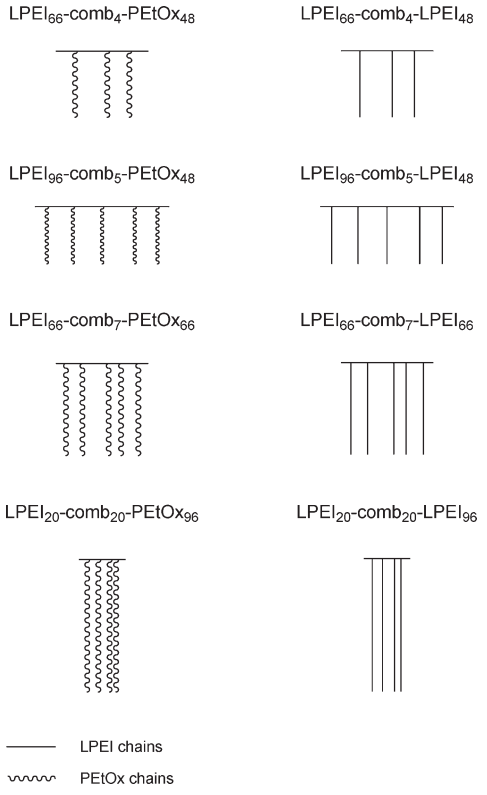

Figure 2. Representation of polymer structures. The structures are not intended to reflect the polymer's conformation in solution.

the branches. Solutions of LPEI-*comb*-PEtOx appeared optically transparent at all temperatures. They remained stable and clear for at least 1 month after preparation. LPEI and LPEI-*comb*-LPEI were initially dissolved by heating the solutions to 60 °C, followed by cooling to 45 °C. The solutions were equilibrated at 45 °C for 15 min and then quickly placed into the DLS holder. The solutions appeared moderately to highly opalescent and only became clear at the highest temperatures tested. DLS measurements were carried out at five different temperatures (25, 35, 45, 55, and 65 °C) for the LPEI-*comb*-PEtOx polymers and at 45, 55, and 65 °C for LPEI and LPEI-*comb*-LPEI polymers. The observation of bi- or trimodal relaxation time distributions made the determination of the static light scattering parameters impossible.

Examples of relaxation time distributions for LPEI, LPEI-*comb*-PEtOx, and LPEI-*comb*-LPEI polymers are shown in Figure 3. The calculated hydrodynamic radii are summarized in Table 3. For LPEI, at 45 °C, along with the fast modes corresponding to particles with dimensions of several nanometers, slow modes of amplitude ≥47% and $R_h^{slow} \geq 155$ nm were also observed. Upon increasing the temperature, however, the slow modes disappeared and distribution was monomodal (see Figure 3a). For both $LPEI_{66}$-$comb_4$-$LPEI_{48}$ and $LPEI_{96}$-$comb_5$-$LPEI_{48}$ the distributions were monomodal at all temperatures tested. At 45 °C large particles with radii of 407 and 899 nm were observed for the solutions of $LPEI_{66}$-$comb_4$-$LPEI_{48}$ and $LPEI_{96}$-$comb_5$-$LPEI_{48}$, respectively, which decreased to 52 and 114 nm upon heating to 65 °C. For the other LPEI-*comb*-LPEI polymers accompanying modes were observed at elevated temperatures (see Figure 3b). Typically, the slow modes featured amplitudes of ≥62% and correspond to particles with dimensions from 82 to 480 nm. Fast particles with $R_h^{fast} \leq 32$ nm and amplitudes ≤6% were responsible for intermediate modes observable at 55 °C. Of particular interest are the fast modes which appeared upon heating the solutions of $LPEI_{20}$ to 55−65 °C. These particles have radii of several nanometers, and it is reasonable to assume that they are unimers. The dissolution of LPEI in water upon heating has been recently described in terms of melting of the hydrated polymer crystals.[22,30] Furthermore, the latest simulation data described the conformation of a linear polymer under poor solvent conditions as a globule of densely packed blobs which unfold in the presence of a good solvent.[51,52] By the use of DLS we are now able to directly monitor the thermal effect upon the LPEI and LPEI-*comb*-LPEI particles in solution and determine the factors that affect the aggregates' stabilities. The data show that upon heating the large particles gradually dissociated into smaller aggregates, their contribution to the scattering light decreases, and eventually the polymers dissolve to unimers. This can be attributed to the weakening of intra- and interchain hydrogen bonds between water and the −NH groups of LPEI[29,30,53] and LPEI-*comb*-LPEI, leading to an increase in the polymer mobility and solubility. Recently, disintegration of large micrometer-size aggregates upon heating has been also reported for the poly(glycidol)-based analogues to the Pluronic block copolymers.[54,55] The disintegration of the large particles has been assigned to the breakdown of the multiple intra- and interchain hydrogen bonds in the poly(glycidol) moieties, either via direct poly(glycidol)−poly(glycidol) interactions or interactions mediated through water molecules. In contrast to $LPEI_{96}$, where the slow particles are still observed at 55 °C, the aggregates formed from $LPEI_{20}$ dissolved at this temperature. This is not surprising, as LPEI crystals of lower molecular weights are known to possess correspondingly lower dissolution temperatures in aqueous solution.[22] Compared to the LPEI aggregates, LPEI-*comb*-LPEI aggregates do not completely dissociate, with the small particles either accompanied by their larger counterparts or else not observed in the solution at all. The particles' size and thermal stability over the entire temperature range were found to decrease in the following order: $LPEI_{96}$-$comb_5$-$LPEI_{48}$ > $LPEI_{66}$-$comb_4$-$LPEI_{48}$ >

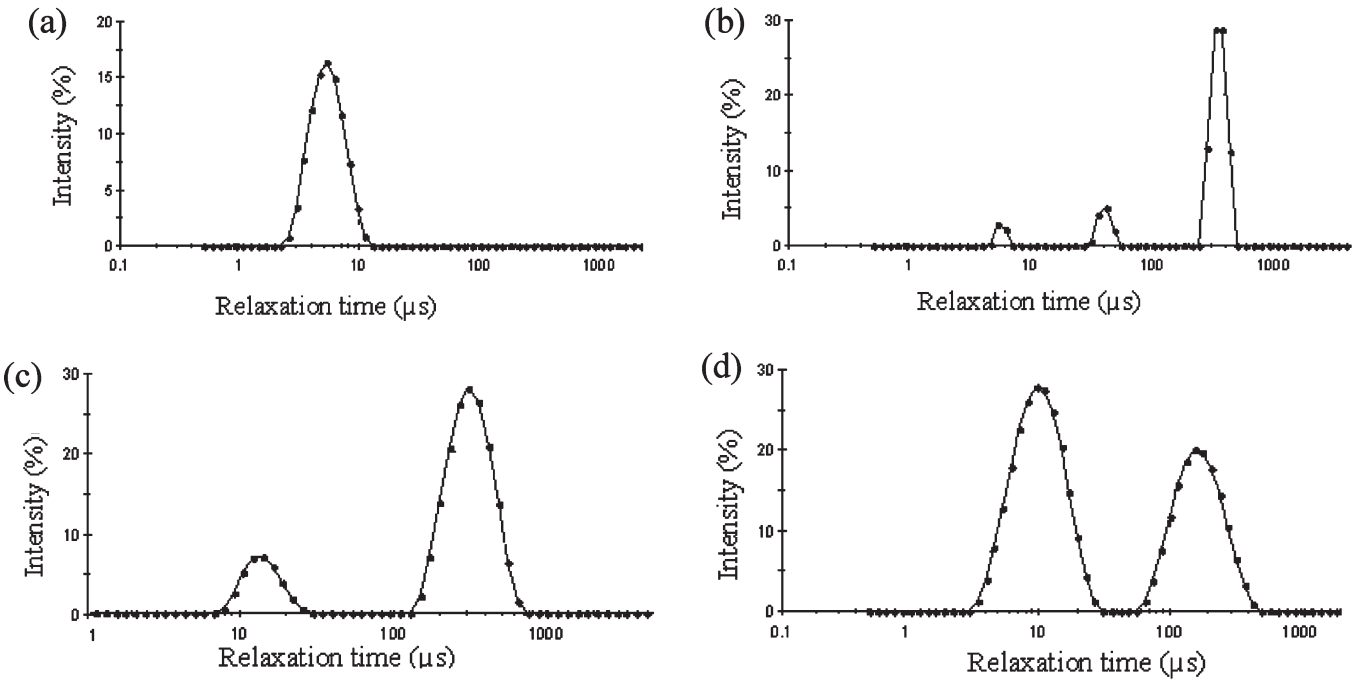

Figure 3. Relaxation time distributions for 3.75 mg mL^{-1} aqueous solutions of (a) $LPEI_{96}$ at 65 °C, (b) $LPEI_{66}$-*comb*$_7$-$LPEI_{66}$ at 55 °C, (c) $LPEI_{66}$-*comb*$_4$-$PEtOx_{48}$ at 25 °C, and (d) $LPEI_{66}$-*comb*$_7$-$PEtOx_{66}$ at 65 °C.

Table 3. Variation of the Hydrodynamic Radius (R_h,[d] in nm) with Temperature for LPEI, LPEI-*comb*-LPEI, and LPEI-*comb*-PEtOx Polymers in Aqueous Solution

	T (°C)				
polymer	25[a]	35[a]	45	55	65
$LPEI_{20}$			*b*		
			$^{47}155$; $^{53}5.1$	0.8	0.8
$LPEI_{96}$			*b*	*b*	
			$^{90}329$; $^{10}5.1$	$^{36}220$; $^{64}4.4$	4.4
$LPEI_{20}$-*comb*$_{20}$-$LPEI_{96}$				*c*	*b*
			247	$^{80}141$; $^{3}14$; $^{17}3.9$	$^{80}82$; $^{20}3.5$
$LPEI_{66}$-*comb*$_7$-$LPEI_{66}$			*b*	*c*	*b*
			$^{91}480$; $^{9}48$	$^{83}277$; $^{6}32$; $^{11}4.5$	$^{62}104$; $^{38}3.4$
$LPEI_{66}$-*comb*$_4$-$LPEI_{48}$			407	247	52
$LPEI_{96}$-*comb*$_5$-$LPEI_{48}$			899	669	114
$LPEI_{20}$-*comb*$_{20}$-$PEtOx_{96}$	*b*	*b*	*b*	*b*	*b*
	$^{40}128$; $^{60}7.3$	$^{42}144$; $^{58}6.3$	$^{48}115$; $^{52}6.4$	$^{47}131$; $^{53}6.3$	$^{45}104$; $^{55}6.2$
$LPEI_{66}$-*comb*$_7$-$PEtOx_{66}$	*b*	*b*	*b*	*b*	*b*
	$^{37}156$; $^{63}12$	$^{29}132$; $^{71}11$	$^{27}142$; $^{73}10$	$^{32}135$; $^{68}9.1$	$^{40}140$; $^{60}8.9$
$LPEI_{66}$-*comb*$_4$-$PEtOx_{48}$	*b*	*b*	*b*	*b*	*b*
	$^{57}110$; $^{43}4.9$	$^{55}114$; $^{45}4.9$	$^{53}127$; $^{47}4.7$	$^{55}124$; $^{55}4.7$	$^{55}99$; $^{55}4.3$
$LPEI_{96}$-*comb*$_5$-$PEtOx_{48}$	*b*	*b*	*b*	*b*	*b*
	$^{58}122$; $^{42}7.3$	$^{55}113$; $^{45}7.2$	$^{53}148$; $^{47}7.3$	$^{49}97$; $^{51}6.6$	$^{49}87$; $^{51}6.4$

[a] No measurements were performed for LPEI and LPEI-*comb*-LPEI at temperatures of 25 and 35 °C. [b] Bimodal distribution. [c] Trimodal distribution. [d] The intensities of the different modes as percentages are presented as superscript on the particles' R_h.

$LPEI_{66}$-*comb*$_7$-$LPEI_{66}$ > $LPEI_{20}$-*comb*$_{20}$-$LPEI_{96}$. The most resistant to heat-induced dissociation are the particles formed of LPEI-*comb*-LPEI polymers with a longer main chain, shorter branches, and lower grafting density (i.e., $LPEI_{96}$-*comb*$_5$-$LPEI_{48}$ and $LPEI_{66}$-*comb*$_4$-$LPEI_{48}$). Although the size of the particles formed from these two polymers is reduced significantly upon heating, at elevated temperatures the relaxation time distributions were still monomodal, implying the presence of large objects with dimensions over 50 nm. However, under the same conditions, the aggregates formed from the remaining two LPEI-*comb*-LPEI

polymers—LPEI$_{66}$-*comb*$_7$-LPEI$_{66}$ and LPEI$_{20}$-*comb*$_{20}$-LPEI$_{96}$—were found to decrease in size to particles with radii of just a few nanometers. The initial temperature increase, from 45 to 55 °C, was found to reduce a larger proportion of the LPEI$_{20}$-*comb*$_{20}$-LPEI$_{96}$ aggregates to relatively smaller particles in comparison with the LPEI$_{66}$-*comb*$_7$-LPEI$_{66}$ aggregates. Moreover, the larger objects in the investigated temperature range were the slow particles for LPEI$_{66}$-*comb*$_7$-LPEI$_{66}$ aqueous solutions. The data imply that the important factors influencing the thermal resistance of the polymer aggregates are the lengths of both the main chain and branches and the grafting density. One explanation for these observations could be that steric repulsion between the branches encourages the heat-induced dissociation, and therefore the particles formed from either less-branched LPEI-*comb*-LPEI polymers or those with shorter branches can be expected to display greater thermal stability.

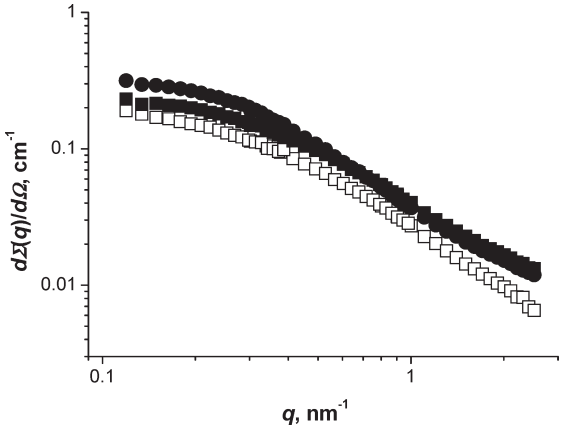

Figure 4. SANS profiles obtained from 3.75 mg mL^{-1} aqueous dispersions of LPEI$_{96}$-*comb*$_5$-PEtOx$_{48}$ (open squares) at 25 °C; LPEI$_{96}$-*comb*$_5$-PEtOx$_{48}$ (closed squares) and LPEI$_{66}$-*comb*$_7$-PEtOx$_{66}$ (closed circle) at 60 °C.

In contrast to LPEI and LPEI-*comb*-LPEI, LPEI-*comb*-PEtOx polymers formed smaller particles in aqueous solution, with smoother temperature variations of R_h^{slow}. The relaxation time distributions were typically bimodal at all temperatures (see Figure 3c,d). The particles responsible for the slow modes are with R_h^{slow} from 87 to 156 nm. The fast modes are with amplitudes approximately equal to or higher than those of the slow modes at elevated temperatures and correspond to particles which cover the R_h^{fast} range from 4.3 to 12.0 nm (see Table 3). It is reasonable to assume that these are dimers, trimers, or slightly larger aggregates. As seen from Table 3, there was no significant alteration in the R_h^{fast} values upon heating the LPEI-*comb*-PEtOx aqueous solution from 55 to 65 °C. It is also important to be emphasized here that in the temperature range studied, although the slow and fast peaks have comparable amplitudes, the concentration of the structures responsible for the slow mode will be considerably smaller.[56,57] For all samples, a decrease in R_h^{slow} was observed with increasing temperature, a feature which correlates well with the increasing solubility of LPEI moieties upon heating. The addition of PEtOx side chains and the accompanying change in macromolecular topology had a dramatic effect on the solubility of the polymer as a whole. Despite the collapsed LPEI backbone at room temperature, the copolymer solutions are stable with respect to microphase separation. The temperature

Table 4. SANS Data of the Particles Formed from LPEI-*comb*-PEtOx Polymers in Aqueous Solutions[a]

		slopes at q ranges					
polymer	T (°C)	0.01−0.03	0.1−0.3	D_{max}, $D_{max,CS}$ (nm)	$I(0)$ (cm^{-1}), $I_{CS}(0)$ (cm^{-1}nm^{-1})	R_g, $R_{CS,g}$ (nm)	r, r_{CS} (nm)
LPEI$_{20}$-*comb*$_{20}$-PEtOx$_{96}$	25	0.61	0.73	15	0.080 ± 0.002	4.76 ± 0.13	6.2
	45	0.60	0.85	15	0.083 ± 0.004	4.65 ± 0.1	6.0
	60	0.53	0.63	15	0.090 ± 0.002	4.46 ± 0.13	5.80
LPEI$_{96}$-*comb*$_5$-PEtOx$_{48}$	25	0.56	1.54	15	0.185 ± 0.002	4.40 ± 0.06	5.70
				3.5	0.011 ± 0.0001	1.15 ± 0.02	1.62
	45	0.54	0.83	15	0.206 ± 0.003	4.41 ± 0.07	5.70
				3.5	0.013 ± 0.0001	1.13 ± 0.02	1.58
	60	0.46	0.69	13	0.209 ± 0.005	3.86 ± 0.06	5.00
				4	0.014 ± 0.0001	1.08 ± 0.02	1.50
LPEI$_{66}$-*comb*$_7$-PEtOx$_{66}$	25	0.60	1.55	15	0.244 ± 0.004	4.62 ± 0.05	6.00
				6	0.014 ± 0.0001	1.57 ± 0.03	2.20
	45	0.60	1.24	15	0.278 ± 0.003	4.59 ± 0.05	5.90
				6	0.016 ± 0.0001	1.55 ± 0.02	2.17
	60	0.49	1.83	15	0.328 ± 0.004	4.54 ± 0.06	5.90
				6	0.019 ± 0.0001	1.57 ± 0.03	2.20
LPEI$_{66}$-*comb*$_4$-PEtOx$_{48}$	25	0.64	1.55	17	0.189 ± 0.004	4.76 ± 0.13	6.10
				3.5	0.011 ± 0.0001	1.06 ± 0.02	1.49
	45	0.60	1.19	17	0.215 ± 0.003	4.74 ± 0.13	6.10
				3.5	0.014 ± 0.0001	1.07 ± 0.02	1.50
	60	0.55	0.82	15	0.212 ± 0.005	4.01 ± 0.1	5.20
				3.5	0.015 ± 0.0001	1.03 ± 0.02	1.45

[a] Slopes of $I(q) \sim q^{-\alpha}$ plots at different q ranges; scattering at "zero angle" $I(0)$ or cross-sectional scattering at zero angle, $I_{CS}(0)$; radius of gyration (R_g) or cross-sectional radius of gyration ($R_{CS,g}$); finite maximum dimensions of the small particles (D_{max}); equivalent sphere radius r or equivalent radius of circular cross section r_{CS} of the aggregates.

dx.doi.org/10.1021/ma2012859 |*Macromolecules* 2011, 44, 7394–7404

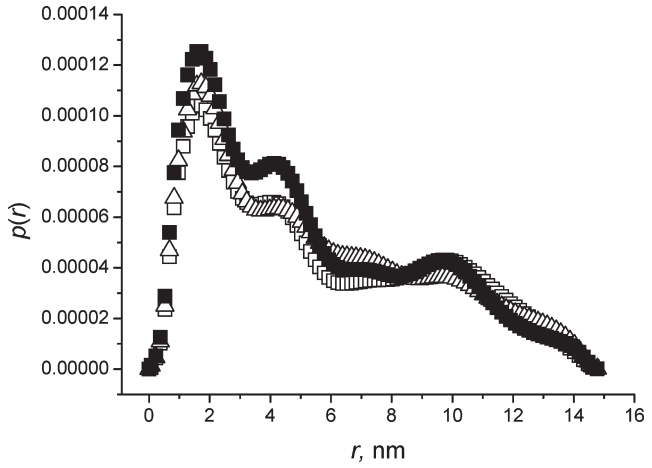

Figure 5. Pair distance distribution function, $p(r)$, obtained from the SANS data of a 3.75 mg mL^{-1} solution of LPEI$_{20}$-*comb*$_{20}$-PEtOx$_{96}$ at 25 °C (open squares), 45 °C (open triangles), and 60 °C (closed squares).

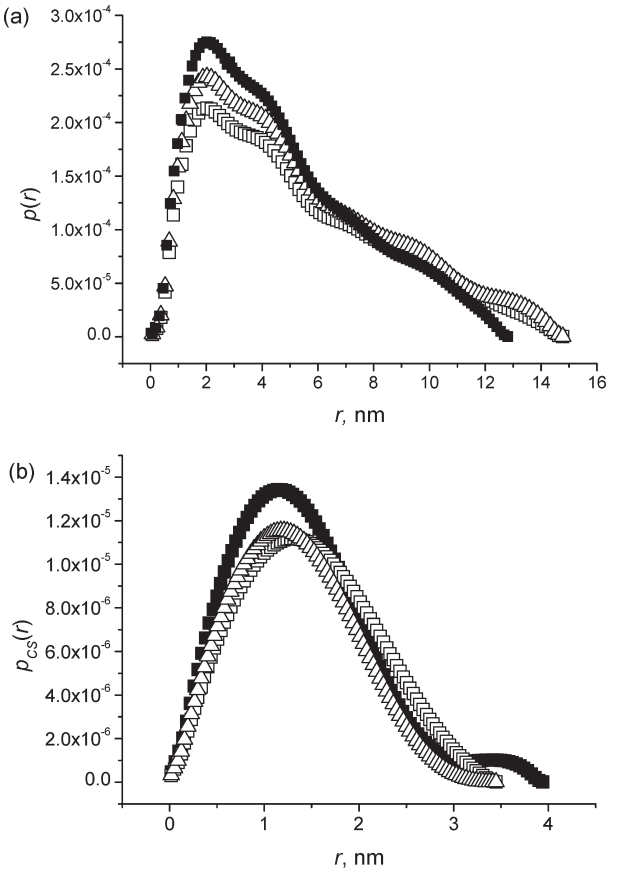

Figure 6. (a) Pair distance distribution function, $p(r)$, and (b) cross-section pair distance distribution function, $p_{CS}(r)$, for a 3.75 mg mL^{-1} solution of LPEI$_{96}$-*comb*$_5$-PEtOx$_{48}$ at 25 °C (open squares), 45 °C (open triangles), and 60 °C (closed squares).

sensitivity of thermosensitive polymers depends upon the extent of the interactions of polymer segments with water via hydrogen bonding. Increasing the temperature weakens the hydrogen bonds between polymer and water molecules, and depending on the hydrophilic/hydrophobic balance of the polymers, a macroscopically observable precipitation at well-defined low critical solution temperature (LCST) can be observed.[58,59] Recently, Weber[40] has studied the aqueous solution behavior of comblike copolymers with hydrophilic oligo(2-ethyl-2-oxazoline) side chains and hydrophobic methacrylate backbones. By incorporating sufficiently low molecular weight PEtOx (which does not feature an LCST) moieties onto a methacrylate backbone, they obtained PEtOx-based comblike polymers which exhibit the LCST behavior of high molecular weight PEtOx. Tuning of the cloud point (CP) by varying molecular weight and composition for other PEtOx-based copolymers has also been achieved.[36,39] LPEI-*comb*-PEtOx polymers do not cloud within the temperature range studied. However, significant dehydration of the PEtOx block is expected at high temperatures.

Comparing the results for the copolymer with the highest (LPEI$_{96}$-*comb*$_5$-PEtOx$_{48}$) and the lowest (LPEI$_{20}$-*comb*$_{20}$-PEtOx$_{96}$) LPEI contents, the larger decrease in R_h^{slow} upon heating was observed for the former polymer (from 122 nm at 25 °C to 87 nm at 65 °C). A similar trend was previously reported for aqueous solutions of poly(*p*-dioxanone)-*graft*-poly(vinyl alcohol) upon heating, where a transition from LCST to upper critical solution temperature (UCST) phase behavior was observed by varying the hydrophobic/hydrophilic balance of the copolymer.[60] In order to investigate the particle structure and possible phase transitions induced by changing solvent strength and how these are affected by the polymer composition, aqueous solutions of the comblike LPEI-based copolymers were further studied by SANS and the results are shown below.

SANS Analysis. SANS experiments were performed at 25, 45, and 60 °C for LPEI-*comb*-PEtOx and 45 °C for some of the LPEI-*comb*-LPEI polymers.

Representative SANS profiles for selected LPEI-*comb*-PEtOx polymers are shown in Figure 4. The scattering data were first analyzed by slope determination (i.e., $I(q) \sim q^{-\alpha}$). The slopes at different q ranges were calculated and selected examples are presented in Table 4. As seen in Figure 4, the scattering curves of the polymers are similar in shape, and at low q range ($q <$ 0.3 nm^{-1}) the scattering from structures with an average radius of 6 nm could be detected. On the q scale of the SANS measurements no traces of scattering from the large LPEI-*comb*-PEtOx particles (seen as a slow mode by DLS) were observed. Therefore, it has been assumed that the main scattering objects in the SANS experiments are the small particles, which were detected as a fast mode by DLS.

The complete q range was analyzed by the indirect Fourier transformation (IFT) approach developed by Glatter[61] and later revised by Pedersen.[62] Previously, IFT has been successfully applied to characterize the aqueous solution properties of a range of polymer and surfactant systems.[54,63,64] Details of this analysis are presented in the Supporting Information. This approach requires only limited information on the possible shapes of the aggregates: spherelike (all three dimensions are of same length scale), rodlike (one size dimension is much larger than the other two), or sheetlike (one dimension is small relative to the other two). Application of IFT enabled us to calculate the shape of the $p(r)$ function (pair distance distribution function); from the $p(r)$ function it is possible to calculate $I(0)$ (scattering at "zero angle") and R_g (radius of gyration of neutron scattering contrast within the aggregate). The values of these two quantities for each polymer are shown in Table 4. At elevated temperatures the scattering contrast of the particles becomes larger (i.e., $I(0)$ increases and R_g decreases upon heating) which could be attributed to polymer dehydration.

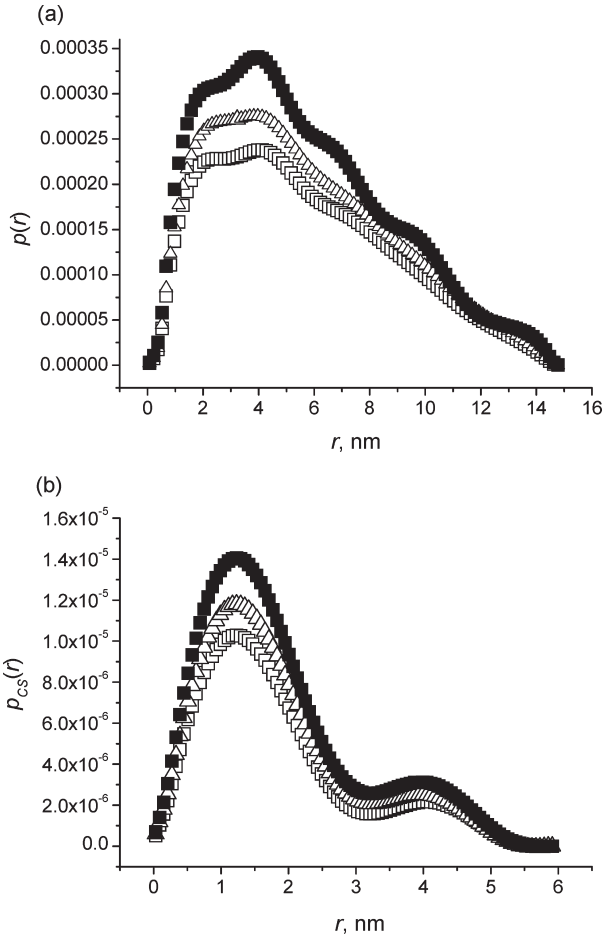

Figure 7. (a) Pair distance distribution function, $p(r)$, and (b) cross-section pair distance distribution function, $p_{CS}(r)$, for 3.75 mg mL^{-1} solutions of LPEI$_{66}$-*comb*$_7$-PEtOx$_{66}$ at 25 °C (open squares), 45 °C (open triangles), and 60 °C (closed squares).

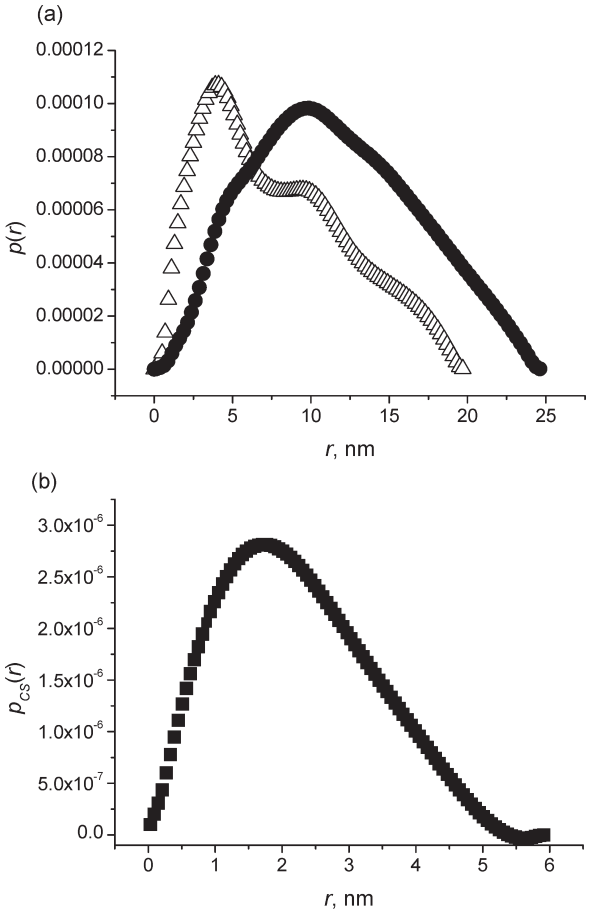

Figure 8. (a) Pair distance distribution function, $p(r)$, for 3.75 mg mL^{-1} solutions of LPEI$_{66}$-*comb*$_7$-LPEI$_{66}$ (open triangles) and LPEI$_{96}$-*comb*$_5$-LPEI$_{48}$ (closed ovals) at 45 °C. (b) Cross-section pair distance distribution function, $p_{CS}(r)$, for a 3.75 mg mL^{-1} solution of LPEI$_{66}$-*comb*$_7$-LPEI$_{66}$ at 45 °C.

LPEI$_{20}$-comb$_{20}$-PEtOx$_{96}$. The scattering curves were analyzed using the IFT model, assuming spherelike geometry. Figure 5 shows the evolution of the $p(r)$ function with temperature for the solution of LPEI$_{20}$-*comb*$_{20}$-PEtOx$_{96}$. The $p(r)$ function is highly asymmetric and displays more than one maximum value within the temperature range tested. The first maximum was attributed to the compact LPEI domains, whereas the second can be attributed to scattering from the corona (presumably consisting of PEtOx branches) which becomes more compact as the temperature increases. The third maximum in $p(r)$ function may be related to the maximum size of the particles, which is ~10 nm (R_h^{fast} ~6 nm, see DLS). Although increasing the temperature did not cause significant alterations in the aggregates' structures, a slight decrease in the total size of the aggregates and a more pronounced level of scattering from their interior was observed.

The R_g values were determined from the second moment of the $p(r)$ functions (Table 4) and are related to both the size of the particles and the distribution of the scattering length density within the particles (see Supporting Information). For homogeneous objects, radii of equivalent spheres, r, could be calculated from R_g, where $r = (5/3)^{1/2}R_g$. For all LPEI-*comb*-PEtOx polymers the values of r are slightly smaller than those of R_h^{fast}, as determined by DLS. This is probably due to the presence of a hydration layer which gives a significant contribution to the DLS results but is almost invisible by SANS.

LPEI$_{96}$-comb$_5$-PEtOx$_{48}$. The scattering data for LPEI$_{96}$-*comb*$_5$-PEtOx$_{48}$, the polymer with the longest LPEI backbone, was analyzed according to the IFT model, assuming spherelike and rodlike geometries. Figure 6a shows the evolution of $p(r)$ function with temperature. At all temperatures, the $p(r)$ function is asymmetric; it decreases gradually at long distances, which implies that the aggregates are anisotropic, presumably rodlike. The scattering intensity for rodlike aggregates can be expressed via a cross-section pair-distance distribution function $p_{CS}(r)$ (see Figure 6b). Its Gaussian shape is characteristic for almost homogeneous, cylindrical crew-cut aggregates. It is reasonable to assume that they are composed of a cylindrical LPEI core surrounded by a thin PEtOx corona. Compared with LPEI$_{20}$-*comb*$_{20}$-PEtOx$_{96}$, the R_g values for LPEI$_{96}$-*comb*$_5$-PEtOx$_{20}$ are somewhat smaller (see Table 4). One possible explanation is the higher contribution of the PEtOx side chains to the scattering for LPEI$_{20}$-*comb*$_{20}$-PEtOx$_{96}$, relative to that of LPEI$_{96}$-*comb*$_5$-PEtOx$_{48}$.

LPEI$_{66}$-comb$_4$-PEtOx$_{48}$ and LPEI$_{66}$-comb$_7$-PEtOx$_{66}$. The aqueous solution behaviors of these polymers are very similar to that observed for LPEI$_{96}$-*comb*$_5$-PEtOx$_{48}$. At all temperatures, the asymmetric shapes of the $p(r)$ functions for LPEI$_{66}$-*comb*$_4$-PEtOx$_{48}$

dx.doi.org/10.1021/ma2012859 |*Macromolecules* 2011, 44, 7394–7404

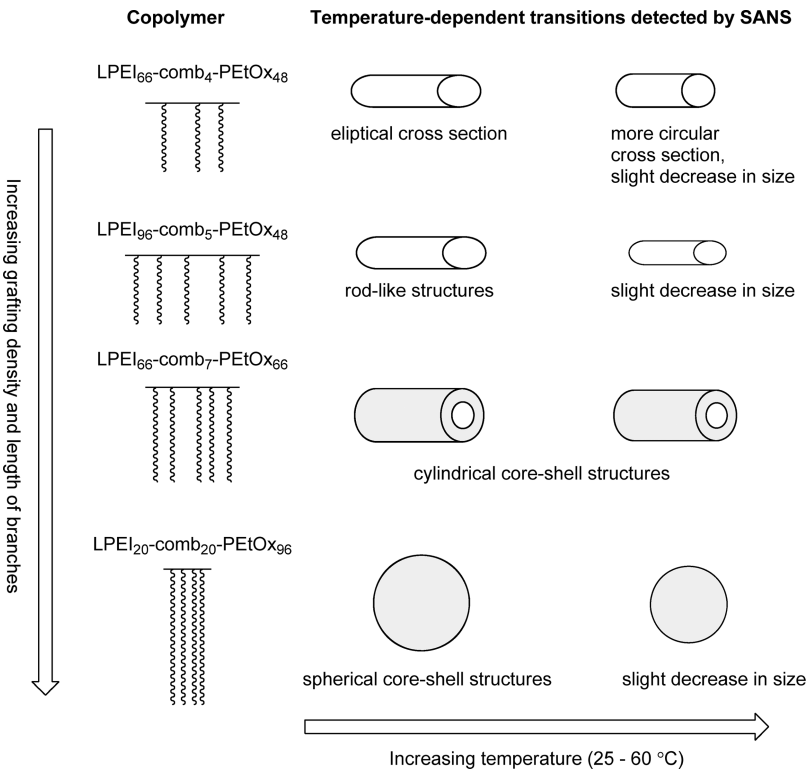

Figure 9. Shape transitions of LPEI-*comb*-PEtOx small particles with temperature and polymer composition. The objects are not drawn to scale.

(see Supporting Information) and $LPEI_{66}$-*comb*$_7$-$PEtOx_{66}$ (Figure 7a) point to an anisotropic shape of the aggregates. Slight decreases in the particle dimensions were observed for $LPEI_{66}$-*comb*$_4$-$PEtOx_{48}$ at elevated temperatures, when the contribution of the core to the overall scattering of the aggregates is increased (Table 4). A further reanalysis by IFT as scattering from rodlike particles gave the $p_{CS}(r)$ functions shown in Figure 7b and in the Supporting Information. The shape of the $p_{CS}(r)$ function for $LPEI_{66}$-*comb*$_4$-$PEtOx_{48}$ is only slightly asymmetric, with a decrease of both cross-section size and asymmetry at high temperatures, suggesting that the cylindrical cross sections of $LPEI_{66}$-*comb*$_4$-$PEtOx_{48}$ aggregates become more compact and closer to circular (see Supporting Information). The $p_{CS}(r)$ function for $LPEI_{66}$-*comb*$_7$-$PEtOx_{66}$ aggregates exhibits two maxima which can be explained by the core−shell model (Figure 7b). The analysis implies that the cylindrical structures consist of a core and shell (the contribution of the shell increases with temperature) and do not exhibit detectable changes in size over the temperature range studied (see Table 4).

LPEI-comb-LPEI Polymers. The $p(r)$ distribution functions for $LPEI_{66}$-*comb*$_7$-$LPEI_{66}$ and $LPEI_{96}$-*comb*$_5$-$LPEI_{48}$ at 45 °C are shown in Figure 8a. For $LPEI_{66}$-*comb*$_7$-$LPEI_{66}$ the corresponding $p(r)$ function is characterized by two maxima at short and long distances, which are attributed to the scattering of the main chain and of the branches, respectively. The particles formed are large, with radii of over 10 nm. The data correlate well with the particle dimensions indicated by DLS. The largest particles are these formed from $LPEI_{96}$-*comb*$_5$-$LPEI_{48}$. The almost-Gaussian shape of the $p(r)$ function for this polymer implies that the particles are compact and close to spherical. The data for $LPEI_{66}$-*comb*$_7$-$LPEI_{66}$ showed values of slopes at low q close to −1, which is characteristic of rodlike objects. IFT analysis for rodlike objects adequately accounted for the data with the $p_{CS}(r)$ function shown in Figure 8b. Its asymmetric shape is indicative of an elliptical cross section for $LPEI_{66}$-*comb*$_7$-$LPEI_{66}$ aggregates.

CONCLUDING REMARKS

A range of LPEI and sparsely grafted, random LPEI-*comb*-PEtOx and LPEI-*comb*-LPEI polymers have been synthesized and their aqueous solution-phase behaviors studied over a range of temperatures. Large particles which tended to decrease in size upon heating were observed in both the LPEI and LPEI-*comb*-LPEI solutions. In contrast to LPEI, the formation of larger and more thermally stable particles was observed in the LPEI-*comb*-LPEI aqueous solutions. The thermal stability was more pronounced for the polymers featuring longer backbones, shorter branches, and lower grafting densities ($LPEI_{96}$-*comb*$_5$-$LPEI_{48}$ and $LPEI_{68}$-*comb*$_4$-$LPEI_{48}$). LPEI-*comb*-PEtOx polymers were found to form smaller aggregates with smoother temperature variations of R_h. The shape and internal structure of the LPEI-*comb*-PEtOx and LPEI-*comb*-LPEI aggregates as well as the temperature evolution of LPEI-*comb*-PEtOx particles were further studied by SANS. The LPEI-*comb*-PEtOx particles (observable as fast modes by DLS) were composed of compact LPEI domains, with PEtOx corona. They also exhibit structural polymorphism, which depends upon the polymer composition. The polymers with low grafting density and short branches form aggregates of anisotropic, rodlike shape ($LPEI_{96}$-*comb*$_5$-$PEtOx_{48}$, $LPEI_{66}$-*comb*$_4$-$PEtOx_{48}$, $LPEI_{66}$-*comb*$_7$-$PEtOx_{66}$), whereas particles featuring a spherical core−shell structure were observed when the polymer was densely grafted, with long branches ($LPEI_{20}$-*comb*$_{20}$-$PEtOx_{96}$, see Figure 9). For $LPEI_{66}$-*comb*$_4$-$PEtOx_{48}$ aggregates, an increase in temperature led to formation of cylindrical aggregates with more compact, nearly circular cross sections. Core−corona type cylindrical aggregates were observed for $LPEI_{66}$-*comb*$_7$-$PEtOx_{66}$

dx.doi.org/10.1021/ma2012859 |*Macromolecules* 2011, 44, 7394–7404

aqueous solutions. In contrast to $LPEI_{66}$-*comb*$_7$-$LPEI_{66}$, where the scattering data were described by assuming rodlike geometry, $LPEI_{96}$-*comb*$_5$-$LPEI_{48}$ formed compact and almost spherical aggregates.

■ ASSOCIATED CONTENT

Supporting Information. Polymer characterization data and SANS analysis data. This material is available free of charge via the Internet at http://pubs.acs.org.

■ AUTHOR INFORMATION

Corresponding Author

*Tel +44 (0)1865 275455; Fax +44 (0)1865 275410; e-mail silviya.halacheva@chem.ox.ac.uk.

■ ACKNOWLEDGMENT

We are grateful to EPSRC for financial support (EP/E029914/1). The SANS study was supported by the European Commission under the sixth Framework Programme through the Key Action: Strengthening the European Research Area, Research Infrastructures (Contract RII3-CT-2003-505925, Grant Agreement No. 226507-NMI3). We thank Dr. Jean van den Elsen from the Department of Biology and Biochemistry at the University of Bath for access to the DLS instrument. We thank Prof. Stanislav Rangelov from the Institute of Polymers, Bulgarian Academy of Sciences, for helpful discussions.

■ REFERENCES

(1) Bajpai, A. K.; Shukla, S. K.; Bhanu, S.; Kankane, S. *Prog. Polym. Sci.* **2008**, *33*, 1088–1118.
(2) Dimitrov, I.; Tzebicka, B.; Muller, A. H. E.; Dworak, A.; Tsvetanov, C. B. *Prog. Polym. Sci.* **2007**, *32*, 1275–1343.
(3) Lowe, A. B.; McCormick, C. L. *ACS Symposium Series 780*; American Chemical Society: Washington, DC, 2001; p 1.
(4) Onaca, O.; Enea, R.; Hughes, D. W.; Meier, W. *Macromol. Biosci.* **2009**, *9*, 129–139.
(5) Forster, S.; Antonietti, M. *Adv. Mater.* **1998**, *10*, 195–217.
(6) Gebhart, C. L.; Kabanov, A. V. *J. Bioact. Biocompat. Polym.* **2003**, *18*, 147–166.
(7) Oerlemans, C.; Bult, W.; Bos, M.; Storm, G.; Frank, J.; Nijsen, W.; Hennik, W. E. *Pharm. Res.* **2010**, 2569–2589.
(8) Schmaljohann, D. *Adv. Drug Delivery Rev.* **2006**, *58*, 1655–1970.
(9) Torchilin, V. P. *Pharm. Res.* **2007**, *24*, 1–16.
(10) Yokoyama, M. *Drug Discovery Today* **2002**, *7*, 426–432.
(11) Blanazs, A.; Armes, S. P.; Ryan, A. J. *Macromol. Rapid Commun.* **2009**, *30*, 267–277.
(12) Borisov, O. V.; Zhulina, E. B. *Macromolecules* **2003**, *36*, 10029–10036.
(13) Borisov, O. V.; Zhulina, E. B. *Macromolecules* **2005**, *38*, 2506–2514.
(14) Kosovan, P.; Kuldova, J.; Limpouchova, Z.; Prochazka, K.; Zhulina, E. B.; Borisov, O. V. *Macromolecules* **2009**, *42*, 6748–6760.
(15) Li, Y.; Ghoreishi, S. M.; Warr, J.; Bloor, D. M.; Penfold, J.; Holzwarth, J. F.; Wyn-Jones, E. *Langmuir* **2001**, *17*, 5657–5665.
(16) Smits, R. G.; Koper, G. J. M.; Mandel, M. *J. Phys. Chem.* **1993**, *97*, 5745–5751.
(17) Koper, G. J. M.; van Duijvenbode, R. C.; Stam, D. D. P. W.; Steuerle, U.; Borkovec, M. *Macromolecules* **2003**, *36*, 2500–2507.
(18) Aoi, K.; Okada, M. *Prog. Polym. Sci.* **1996**, *21*, 151–208.
(19) Kobayashi, S.; Uyama, H. *J. Polym. Sci., Part A* **2002**, *40*, 192–209.
(20) Jeong, J. H.; Song, S. H.; Lim, D. W.; Lee, H.; Park, T. G. *J. Controlled Release* **2001**, *73*, 391–399.
(21) Kem, K. M. *J. Polym. Sci., Part A: Polym. Chem.* **1979**, *17*, 1977–1990.
(22) Lambermount-Thijs, H. M.; van der Woerdt, F. S.; Baumgaertel, A.; Bonami, L.; Du Prez, F. E.; Schubert, U. S.; Hoogenboom, R. *Macromolecules* **2010**, *43*, 927–933.
(23) Tanaka, R.; Ueoka, I.; Takaki, Y.; Kataoka, K.; Saito, S. *Macromolecules* **1983**, *16*, 849–853.
(24) Saegusa, T.; Ikeda, H.; Fujii, H. *Macromolecules* **1972**, *5*, 108–108.
(25) Chatani, Y.; Kobatake, T.; Tadokoro, H. *Macromolecules* **1983**, *16*, 199–204.
(26) Chatani, Y.; Kobatake, T.; Tadokoro, H.; Tanaka, R. *Macromolecules* **1982**, *15*, 170–176.
(27) Chatani, Y.; Tadokoro, H.; Saegusa, T.; Ikeda, H. *Macromolecules* **1981**, *14*, 315–321.
(28) Hashida, T.; Tashiro, K.; Aoshima, S.; Inaki, Y. *Macromolecules* **2002**, *35*, 4330–4336.
(29) Kakuda, H.; Okada, T.; Otsuta, M.; Katsumoto, Y.; Hasegawa, T. *Anal. Bioanal. Chem.* **2009**, *393*, 367–376.
(30) Kakuda, H.; Okada, M.; Hasegawa, T. *J. Phys. Chem. B* **2009**, 13910–13916.
(31) Griffiths, P. C.; Alexander, C.; Nilmini, R.; Pennadam, S. S.; King, S. M.; Heenan, R. K. *Biomacromolecules* **2008**, *9*, 1170–1178.
(32) Hsiue, G. H.; Chiang, H. Z.; Wang, C. H.; Juang, T. M. *Bioconjugate Chem.* **2006**, *17*, 781–786.
(33) Petersen, A.; Fechner, P. M.; Martin, A. L.; Kunath, K.; Stolnik, S.; Roberts, C. J.; Fischer, D.; Davies, M. C.; Kissel, T. *Bioconjugate Chem.* **2002**, *13*, 845–854.
(34) Wang, H.; Chen, X.; Pan, C. *J. Colloid Interface Sci.* **2008**, *320*, 62–69.
(35) Zhong, Z.; FeijenMartin, J.; Lok, C.; HenninkLane, V. C.; Yockman, J. W.; Kim, Y. H.; Kim, A. W. *Biomacromolecules* **2005**, *6*, 3440–3448.
(36) Hoogenboom, R. *Angew. Chem., Int. Ed.* **2009**, *48*, 7978–7994.
(37) Adams, N.; Schuber, U. S. *Adv. Drug Delivery Rev.* **2007**, *59*, 1504–1520.
(38) Christova, D.; Velichkova, R.; Loos, W.; Goethal, E. J.; Du Prez, F. *Polymer* **2003**, *44*, 2255–2261.
(39) Hoogenboom, R.; Thijs, H. M. L.; Jochems, M. J. H. C.; van Lankvelt, B. M.; Fijten, M. W. M.; Schuber, U. S. *Chem. Commun.* **2008**, 5758–5760.
(40) Weber, C.; Becer, C. R.; Hoogenboom, R.; Schuber, U. S. *Macromolecules* **2009**, *42*, 2965–2971.
(41) Tomalia, D. A.; Hedstrand, D. M.; Feritto, M. S. *Macromolecules* **1991**, *24*, 1435–1438.
(42) Hedstrand, D. M.; Tomalia, D. A.; Yin, R. US Pat. No. WO/1996/022321, 1996.
(43) Halacheva, S.; Rangelov, S.; Tsvetanov, C. *J. Phys. Chem. B* **2008**, *112*, 1899–1905.
(44) Rathbone, S. J.; Haynes, C. A.; Blanch, H. W.; Prausnitz, J. M. *Macromolecules* **1990**, *23*, 3944–3947.
(45) Ogura, M.; Tokuda, H.; Imabayashi, S.; Watanabe, M. *Langmuir* **2007**, *23*, 9429–9434.
(46) Stuhrmann, H. B.; Burkhardt, N.; Dietrich, G.; Junemann, R.; Meerwinck, W.; Scmitt, M.; Wadzak, J.; Willumeit, R.; Zhao, J.; Nierhaus, K. H. *Nucl. Instrum. Methods* **1995**, *A356*, 133–137.
(47) Pedersen, J. S.; Posselt, D.; Mortensen, K. *J. Appl. Crystallogr.* **1990**, *23*, 321–333.
(48) Aoi, K.; Takasu, A.; Okada, M. *Macromol. Chem. Phys.* **1994**, *195*, 3835–3844.
(49) Stawski, D.; Halacheva, S.; Bellmann, S.; Simon, F.; Polowinski, S.; Price, G. *J. Adhesion Sci. Technol.* **2011**, *25*, 1481–1495.
(50) Brissault, B.; Kichler, A.; Guis, C.; Leborgne, C.; Danos, O.; Cheradame, H. *Bioconjugate Chem.* **2003**, *14*, 581–587.
(51) Halperin, A.; Zhulina, E. B. *Europhys. Lett.* **1991**, *15*, 417–421.
(52) Dobrynin, A. V.; Rubinstein, M.; Obukhov, S. P. *Macromolecules* **1996**, *29*, 2974–2979.

(53) Kokufuta, E.; Suzuki, H.; Yoshida, R.; Yamada, K.; Hirata, M.; Kaneko, F. *Langmuir* **1998**, *14*, 788–795.
(54) Halacheva, S.; Rangelov, S.; Garamus, V. M. *Macromolecules* **2007**, *40*, 8015–8021.
(55) Rangelov, S.; Almgren, M.; Halacheva, S.; Tsvetanov, C. *J. Phys. Chem. C* **2007**, *111*, 13185–13191.
(56) Alami, E.; Almgren, M.; Brown, W. *Macromolecules* **1996**, *29*, 2229–2243.
(57) Rangelov, S.; Dimitrov, P.; Tsvetanov, C. *J. Phys. Chem. B* **2005**, *109*, 1162–1167.
(58) Schild, H. G. *Prog. Polym. Sci.* **1992**, *17*, 163–249.
(59) Chen, S. C.; Wilson, J.; Chen, W.; Davis, R. M.; Riffle, J. S. *Polymer* **1994**, *35*, 3587–3591.
(60) Wu, G.; Chen, S. C.; Zhan, Q.; Wang, Y. Z. *Macromolecules* **2011**, *44*, 999–1008.
(61) Glatter, O. *J. Appl. Crystallogr.* **1977**, *10*, 415–421.
(62) Hansen, S.; Pedersen, J. S. *J. Appl. Crystallogr.* **1991**, *24*, 541–548.
(63) Almgren, M.; Garamus, V. M.; Asakawa, T.; Jiang, N. *J. Phys. Chem. B* **2007**, *111*, 7133–7141.
(64) Rangelov, S.; Halacheva, S.; Garamus, V. M.; Almgren, M. *Macromolecules* **2008**, *41*, 8885–8894.